Olga Laurmania Quevedo Pinos,[1,5]* Tyrone Fernando Alcívar Reyna,[1,2] Kevin Nivaldo Zamora Murillo,[1]
Rosa María Cerón Bretón,[3] Julia Griselda Cerón Bretón,[3] Ariel René Baque Onofre,[4]
and Ninozka Leslye Veliz Saltos[1]

[1]Universidad de Guayaquil. Guayaquil, Ecuador. olga.quevedop@ug.edu.ec, kevin.zamoram@ug.edu.ec. leslye.velizs@ug.edu.ec
[2]Escuela Superior Politécnica del Litoral (ESPOL). Guayaquil, Ecuador. talcivar@espol.edu.ec.
[3]Universidad Autónoma del Carmen. Ciudad del Carmen, Campeche, México. rceron@pampano.unacar.mx, jbreton@delfin.unacar.mx.
[4]Industria Pesquera Santa Priscila. Guayaquil, Ecuador. ariel.baqueo@ug.edu.ec.
[5]Universidad Técnica Estatal de Quevedo. Quevedo, Los Ríos, Ecuador. oquevedop@uteq.edu.ec.

*Corresponding author: olga.quevedop@ug.edu.ec.

Received: 05/03/2025. **Last review:** 20/06/2025. **Accepted:** 09/10/2025.

Applied and Analytical

Stoichiometric Validation of Sulfur Sulfates in Guayaquil, Ecuador, during 2018 and 2019

Abstract

Sulfur (S) is used by many industries in the city of Guayaquil as an additive, intermediate product or raw material. However, their management can cause environmental impacts and respiratory health problems. The purpose of this study was to perform a stoichiometric analysis of the critical loads of atmospheric S deposits present in Guayaquil, Ecuador. Data was collected between 2018 and 2019 in 16 sites with high anthropogenic activity, the data was obtained with the application of passive samplers or throughfall traps. Stoichiometric reactions were then applied to recognize the concentrations of the analyte in the atmosphere and the impact it causes. The results showed that the oxidation of sulfur dioxide (SO_2) generates sulfur trioxide (SO_3) in concentrations from 0.2285 to 0.7326 g. Likewise, between 1.36×10^{-3} and 6.35×10^{-3} g of sulfuric acid (H_2SO_4) were formed during the washing process, corresponding to the dry and rainy seasons in which the samples were collected, respectively. It was concluded that the SO_2 present in the atmosphere undergoes changes when captured by the samplers, influenced by the different oxidative states of the S.

Keywords: environmental impact; reactions; analyte; sulfate ion; samplers.

Validación estequiométrica de sulfatos de azufre en Guayaquil, Ecuador, durante 2018 y 2019

Resumen

El azufre (S) es utilizado por muchas industrias en la ciudad de Guayaquil como aditivo, producto intermedio o materia prima; sin embargo, su manejo puede provocar impactos ambientales y causar problemas de salud respiratoria. El objetivo de este estudio fue realizar un análisis estequiométrico de las cargas críticas de los depósitos atmosféricos de S presentes en Guayaquil, Ecuador. Para ello se utilizaron datos recolectados entre 2018 y 2019 en 16 sitios con una alta actividad antropogénica, los datos se obtuvieron con la aplicación de muestreadores pasivos o trampas throughfall. Después se aplicaron reacciones estequiométricas para reconocer las concentraciones del analito en la atmósfera y el impacto que provoca. Los resultados mostraron que la oxidación del dióxido de azufre (SO_2) genera trióxido de azufre (SO_3) en concentraciones que varían entre 0,2285 y 0,7326 g. Asimismo, durante el proceso de lavado se formaron entre $1,36 \times 10^{-3}$ y $6,35 \times 10^{-3}$ g de ácido sulfúrico (H_2SO_4), correspondientes a las épocas seca y lluviosa en las que se recolectaron las muestras, respectivamente. Se concluyó que el SO_2 presente en la atmósfera sufre cambios al ser captado por los muestreadores, influenciado por los diferentes estados oxidativos del S.

Palabras clave: impacto ambiental; sulfatos del azufre; contaminación atmosférica.

Validação estequiométrica dos sulfatos de enxofre na Guayaquil, Equador, durante 2018 e 2019

Resumo

O enxofre (S) é utilizado por muitas indústrias na cidade de Guayaquil como aditivo, produto intermediário ou matéria-prima; no entanto, seu manuseio pode causar impactos ambientais e causar problemas de saúde respiratória. O objetivo deste estudo foi realizar uma análise estequiométrica das cargas críticas dos depósitos atmosféricos de S presentes em Guayaquil, Equador. Foram utilizados dados coletados entre 2018 e 2019 em 16 locais com alta atividade antrópica, os dados foram obtidos com a aplicação de amostradores passivos ou armadilhas de precipitação. Reações estequiométricas foram então aplicadas para reconhecer as concentrações do analito na atmosfera e o impacto que ele causa. Os resultados mostraram que a oxidação do dióxido de enxofre (SO_2) gera trióxido de enxofre (SO_3) em concentrações de 0,2285 a 0,7326 g. Da mesma forma, entre $1,36 \times 10^{-3}$ e $6,35 \times 10^{-3}$ g de ácido sulfúrico (H_2SO_4) foram formados durante o processo de lavagem, correspondendo às estações seca e chuvosa em que as amostras foram coletadas, respectivamente. Concluiu-se que o SO_2 presente na atmosfera sofre alterações quando capturado pelos amostradores, influenciado pelos diferentes estados oxidativos do S.

Palavras-chave: impacto ambiental; reações; analito; íons sulfato; amostradores.

Introduction

Environmental pollution significantly affects urban areas, which are directly exposed to the combustion gases resulting from traffic congestion [1]. This pollution adversely impacts the health of residents [2] and specifically causes harm by degrading soil quality [3], leading to potential issues such as acidification [4]. This article highlights the extent of this pollution by applying material balance concepts and examining the chemical reactions involved in these processes [5], while considering various factors such as gas emissions from the burning of fossil fuels across different industries, including textiles, steel, shipping, and vehicular traffic. These activities contribute to both dry and wet sulfur (S) deposits.

In the port city of Guayaquil [6], within the mangrove ecosystem, high concentrations of S have been reported, exceeding the threshold for sensitive ecosystems at 7,45 kilograms per hectare per year (kg ha^{-1} $year^{-1}$) [7]. These processes lead to eutrophication, which affects the environment by depositing S and nitrogen (N) compounds that acidify both aquatic and terrestrial ecosystems [8].

Suspended particles, or atmospheric aerosols, are complex mixtures that have different compositions and sizes. These particles can be produced by both human activities and natural sources [9]. As they travel through the atmosphere, sulfur dioxide (SO_2) and its oxidation products react with oxygen and water vapor, creating strong acids such as sulfuric acid ($H_2 SO_4$). This acid falls to the earth as rain, snow, or fog, a phenomenon known as acid deposition [10].

Forest ecosystems, such as mangroves, are often surrounded by industries that have a negative impact on soil quality. These industries include liquefied gas bottling plants, thermoelectric plants, and ports, all of which are located within or on the boundaries of protected natural areas in urban settings [11]. Previous studies on the S deposits in the port of Guayaquil indicate that this area is affected by a uniform distribution of these deposits within a 40 km radius [12]. The cities of Durán and Guayaquil are adjacent to each other, separated only by the Guayas River. They experience heavy vehicular traffic because this region serves as a vital connection point between the mountains and the coast. The industrial park in these areas comprises approximately 300 industries spread over about 500 ha.

The vegetation in the protected areas of Isla Santay and Estero Salado, located in the cantons of Durán and Guayaquil, respectively, can be influenced by S deposits. While S can have beneficial effects on plant productivity in moderate amounts [13], excessive quantities may harm plant development [14]. A similar issue arises with soil acidification. To assess the potential damage caused by S deposition on both the soil and vegetation in the study area, various models have been developed [15].

As Darmstaedter and Oesper mention [16], matter balances can be effectively used to predict the required amounts of various components needed to prepare a formulation of food or drugs based on their composition. This research builds on that concept. Matter balance is defined as the accounting of inputs and outputs in a process, adhering to the law of conservation of mass proposed by the French scientist Antoine Lavoisier in 1785.

To achieve an accurate balance, it is essential to identify the reactions involved in the process. This implies applying stoichiometric calculations based on established principles [17]. The aim is also to provide new scientific contributions supported by important calculation procedures in the study of chemical reactions.

This research aims to prove the amount of sulfate (SO_4^{2-}) (from atmospheric deposition) that settles on the ground through stoichiometric calculations in mass units. It corroborates these estimates with matter balances for each of the involved processes, enhancing the reliability of the critical loads for S deposition obtained in the Port of Guayaquil during 2018 and 2019.

Materials and methods

Passive Samplers

Passive samplers, often referred to as throughfall samplers, enable the evaluation of critical areas over extended periods due to their simple construction, installation, and maintenance. They do not require any pumping systems or electrical power. This cost-effective method is especially recommended for establishing a dense surveillance network with multiple key collection points or sites [18]. In this study, S deposition fluxes were estimated by using Ionic Exchange Resin (IER) columns. While this methodology enables the simultaneous determination of N and S at multiple points economically, the study's objective was to measure atmospheric deposition levels of SO_4^{2-} and characterize deposition gradients and trends in the mangrove forest surroundings and downwind of some industrial zones in the port of Guayaquil. However, it is necessary to point out that this methodology has already been tested and validated by Fenn *et al.* [19]. Therefore, a standardized protocol for installation and exposure was implemented, utilizing replicates at selected sites. The average standard deviation observed between pairs of samplers installed in parallel was 7.3%, which aligns with the levels of uncertainty anticipated in passive sampling methods [20].

The widespread application of the IER method is promising because it allows for the measurement of accumulated deposition over extended periods, potentially up to a year [21]. This significantly reduces the sampling effort required in the field and the number of laboratory analyses needed, resulting in considerable cost savings [22–24]. Additionally, the IER method can measure deposition in areas with low rainfall or low elemental concentrations, thus avoiding issues related to detection limits and the minimal sample size required in the bulk deposition method [23]. The following section provides a detailed description of how the sampling device was configured.

Resin Selection

The resin used in IER collectors was an anion and cation exchange resin with mixed bed (Amberlite™ IRN150). Regarding this, some researchers have evaluated various IER and extraction solutions to identify the most suitable options for studying atmospheric throughfall deposition, depending on the specific species being analyzed. Amberlite IRN 150 has a well-balanced blend of strong cationic and anionic resins. This enables it to retain N ions, such as ammonium (NH_4^+) and nitrate (NO_3^-), and S ions, such as SO_4^{2-}, simultaneously.

Unlike other resins that require pairing for the same function, such as Amberlite IR-120 (cationic) and IRA-400 (anionic), Amberlite IRN 150 simplifies logistics in the field by combining these capabilities into one product. This resin exhibits good resistance to variations in temperature, humidity, and pH, making it suitable for long-term passive collectors. In contrast, more selective resins may degrade faster or lose efficiency in humid or acidic tropical environments. Although Amberlite may be more expensive than some single-type resins, its dual functionality offsets the costs by reducing the need for handling and allowing for a single extraction step [18, 25–26]. According to the above, Fenn *et al.* recommend using Amberlite™ IRN 150 to collect N and S atmospheric deposition [18].

Ionic Exchange Resin (IER) Sampling Device Configuration

For each column (made from 1.27 cm diameter PVC tubing), 35 g of Amberlite IRN™ 150 resin was added and rinsed with distilled water. This amount of resin is consistent with that used in a previous study [19]. According to Fenn *et al.* [18], based on their former throughfall studies and the ion exchange capacity of the resin, 35 g is more than sufficient for the ion exchange capacity required for throughfall collection at the study sites.

To facilitate the operation of the columns, glass wool was inserted at the top and bottom. The bottom was sealed with a slit cap to allow the throughfall solution to percolate through. The throughfall solution, or precipitation samples, were collected using funnels like those found in conventional throughfall samplers. However, in this case, the solution was allowed to drain through the resin column where the ions were adsorbed by the ion-exchange resin. Background levels of NO_3^- and SO_4^{2-} in the resin columns were determined by extracting the columns three times with 200 mL of 2 N KCl. **Figure 1** shows a photograph of the IER device configuration used for the deposition sampling in this study.

Figure 1. Ion Exchange Resin (IER) sampling devices used in this study.

Table 1. Sampling sites chosen for this study, with their respective coordinates.

Sampling sites			
N°	**Name**	**Coord-X**	**Coord-Y**
1	Trinitaria	620530.80	9750011.00
2	Acacias	621913.34	9754526.36
3	Autoridad Portuaria de Guayaquil	621974.50	9747844.00
4	Isla Trinitaria (COGUAR)	619541.70	9748739.00
5	Floresta 3	623194.70	9749971.61
6	Isla Santay - Durán	627179.92	9758098.01
7	Primavera I	629111.67	9761154.46
8	El recreo	633590.15	9759899.34
9	San Eduardo	619150.26	9758308.61
10	Parque Forestal	622811.70	9757527.00
11	Instituto de Investigaciones UG	622057.16	9759235.93
12	Terranostra	611079.60	9758312.41
13	Terminal Tres Bocas	615791.20	9753513.00
14	Cantera Eva Adriana	613150.89	9758658.46
15	Chongón	602451.95	9753301.68
16	Colegio Cenest Harvard	612201.00	9758820.00

The IER column design used in this study offers several advantages. First, the resin doesn't contact the ground nor forest floor, ensuring that the solution has improved access to the ion exchange resin. Additionally, the resin can be easily extracted from the same columns used during the field exposure by percolating 200 mL of 2 N KCl solution through the intact resin columns.

Fenn *et al.* [19] found that prerinsing the columns with 100 mL of distilled water before the potassium chloride (KCl) extractions leads to a more efficient and consistent extraction process. The columns were extracted three times, with 200 mL used for each extraction. However, it soon became evident that the amount of N and S removed in the second and third extractions was minimal. In these later extracts, concentrations of SO_4^{2-} and NO_3^- were frequently close to detection limits [27].

Extraction Efficiency

Studies that report on adsorption capacity primarily focus on a limited number of elements tested in laboratory conditions [28–30]. In contrast, recovery efficiency is frequently documented under these same conditions, typically showing high recovery rates ranging from 87 to 100% [21]. The adsorption capacity and recovery efficiency can be affected by environmental conditions such as drought, frost, or high temperatures [31–32]. However, there are very few studies that have investigated the impact of these environmental factors on the adsorption capacity and recovery efficiency of the resin.

The effectiveness of the IER method for measuring a wide range of elements relies on the performance of the resin. This performance is evaluated in two keyways: first, by the adsorption capacity, which is the percentage of the total element flux that the resin can bind; and second, by the recovery efficiency, which indicates the percentage of the total element flux that can be recovered from the resin [30]. To evaluate the recovery efficiency of the devices proposed by Fenn *et al.* [19], we conducted two separate tests. One test was based on the findings reported by Simkin *et al.* [28], while the other followed Fenn's suggestions [19]. In both instances, we achieved high recovery efficiencies for both NO_3^- and SO_4^{2-}. The results were consistent with those noted in the literature.

An extraction efficiency test, like the one conducted by Simkin *et al.* [28], was performed. Our results indicated that using 200 mL of 2 N KCl for extracting resin columns was sufficient to recover at least 96% of SO_4^{2-} from all treatments (see **Table 2**). These findings align with the results reported by Simkin *et al.* [28].

Table 2. Experimental design to test the recovery efficiency of Ion Exchange Resin (IER) columns.

	SO_4^{2-}	
Treatment (µEq)	**Recovery (%)**	**CV (%)**
50	98.70	0.82
125	98.60	3.02
250	97.41	1.31
500	96.8	0.35
2500	95.73	0.87
5000	96.43	0.79

The extraction efficiency for the 50 and 125 µeq anion treatments was nearly 100%, while recovery decreased slightly as the loading increased. All data were adjusted by subtracting the blank values from the raw measurements. The average blank value measured for SO_4^{2-} was 1.032 µeq (± 0.29). This blank value accounts for nearly 2% of the lowest loading level (50 µeq) but represents less than 0.02% of the highest loading level (5000 µeq). However, it is essential to recognize that the accuracy of this blank value is limited, as it was close to the method's detection limit.

In addition, we conducted laboratory tests like those described by Fenn *et al.* [19] using resin columns that were preloaded with a simulated throughfall solution. This solution had a deposition rate

equivalent to 120 kg of SO_4^{2-} per hectare, allowing us to evaluate the recovery efficiency of the adsorbed ion. Five columns were preloaded with a specific amount of SO_4^{2-} in the simulated throughfall solution, and the experiment was repeated with consistent results. The preloading rate was determined based on the highest reported deposition rates of SO_4^{2-} in various locations around the world. The laboratory tests revealed that at least 97.1% of the SO_4^{2-} was extracted during the first extraction (see **Table 3**). These findings closely align with those reported [19].

Table 3. Laboratory test of ion extraction procedure from Ion Exchange Resin (IER) column.

SO_4^{2-} ion recovery from resin columns			
	After the first extraction	After the second extraction	After the third extraction
Percent	97.10	100.3	101.5
Standard error of the mean (n = 5)	1.2	1.2	1.2

Extraction and Analysis Procedure

Quality control measures in this study included a blank IER tube that was capped and deployed on-site for the same duration as the other tubes, as well as an analysis of laboratory standards and random duplicate samples. In the laboratory, we began by removing the glass wool from the top end of the PVC tube and then adding a 30 cm extension of PVC pipe. We closed the bottom valve and positioned the system on a universal stand. Next, we poured 200 mL of distilled water into each sampler and allowed it to sit for 20 min to help dissolve any soluble residues.

After this, we opened the bottom valve to let the wash water flow at a consistent rate of two drops per second for 10 min; this initial eluent was discarded. Following this, we performed a second elution using 200 mL of a 2 N KCl solution, which was prepared by diluting a 149.1 mg L^{-1} stock solution to 1 L. This solution was collected at the same drop rate. We collected approximately 200 mL of the resulting volume into polyethylene bottles, which were then refrigerated until analysis.

SO_4^{2-} analysis was conducted according to the procedure outlined in the Mexican standard NMX-AA-074-1981 [32]. To quantify SO_4^{2-}, a conditioning solution was prepared, consisting of 50 mL of glycerol, 30 mL of concentrated hydrochloric acid (HCl), 300 mL of water, 100 mL of 95% ethyl (or isopropyl) alcohol, and 75 g of sodium chloride. For the analysis, 2 mL of this conditioning solution and a teaspoon of barium chloride ($BaCl_2$) crystals were added to 40 mL of the eluate from each sample. The mixture was stirred magnetically, and after one minute of reaction time, the resulting turbidity was measured using a THERMO Genesys 10 UV-Vis spectrophotometer at a wavelength of 420 nm. Readings were recorded every 30 seconds for a duration of 4 min. A calibration curve was constructed using standard SO_4^{2-} solutions, resulting in a correlation coefficient of $R^2 = 0.9813$.

Estimation of Atmospheric Deposition Fluxes of Sulfate (SO_4^{2-})

Atmospheric deposition fluxes of SO_4^{2-} were determined by extrapolating from the area of the collector opening and the amounts of inorganic S that were extracted from the IER columns [22].

Retrospective Description

As part of the FCI 0018 project, 16 passive samplers were deployed in the vicinity of Estero Salado (**Figure 2**), located near the maritime port of Guayaquil, during the period from 2018 to 2019. These passive devices (IER samplers) were deployed to capture the S atmospheric deposition over a period of 22 to 30 days.

Figure 3 illustrates the descriptive statistics for S deposition fluxes, measured as SO_4^{2-} in kg ha^{-1} $year^{-1}$. These fluxes were determined from SO_4^{2-} concentration in resin extracts, considering the funnel catchment area and the collection time [33]. The highest S deposit values were recorded at the port of Guayaquil (5.0 kg ha^{-1} $year^{-1}$), located in the southern part of the city. Surrounding neighborhoods such as Las Acacias, Puerto Guayaquil, Coguar, and Parque Forest also show similar levels, averaging 3.82 kg ha^{-1} $year^{-1}$, as illustrated in **Figure 3**. In contrast, the lowest S deposit values were found to the north of the city along the coastal highway, as well as in areas with natural vegetation, which exhibit significantly lower levels compared to the urban shipping and industrial zones in the south of the city.

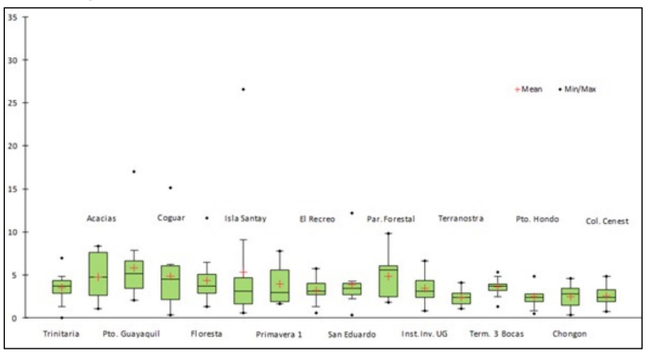

Figure 3. Descriptive statistics of atmospheric sulfur (S) deposition fluxes (kg ha^{-1} $year^{-1}$) at the 16 study sites in the mangroves of El Salado, Guayaquil, Ecuador, during the period from May 2018 to April 2019.

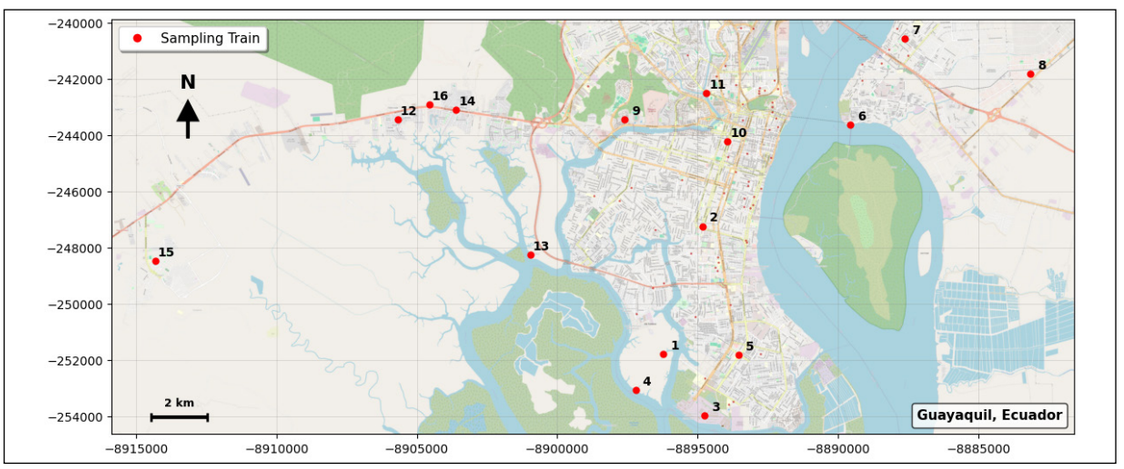

Figure 2. Geographic location of the sites for measuring sulfur (S) in dry and wet deposits within the mangroves of El Salado, Guayaquil, Ecuador. Made in Google Earth, 2023.

Spatial analysis identified critical zones of S deposition (samples 15 and 40) with fluxes exceeding 25 kg ha^{-1} year^{-1} during the rainy season of 2019, and significant peaks were observed during the dry season of 2018. These zones were primarily located in industrial, urban, and port areas of Guayaquil. In contrast, other locations showed more consistent and considerably lower values (≤ 7 kg ha^{-1} year^{-1}), highlighting the spatial heterogeneity of contamination.

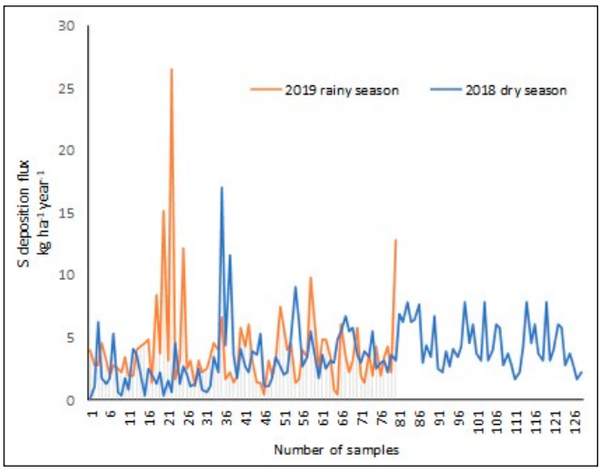

Figure 4. Sulfur (S) concentrations during the dry and rainy seasons from 2018 to 2019, at 16 sampling sites in the city of Guayaquil.

The temporal analysis (**Figures 4** and **5**) indicates a trend of increased atmospheric S deposition during the dry months, specifically from August to December, with average values approaching 6 kg ha^{-1} year^{-1}. In contrast, during the rainy months, the concentrations were more variable, featuring specific events of high deposition. These observations lead us to conclude that the passive methodology employed is both efficient and low-cost, making it suitable for characterizing spatiotemporal patterns in complex urban environments. This validates its applicability in extensive monitoring networks.

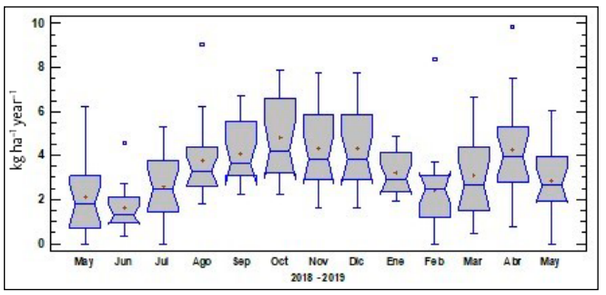

Figure 5. Annual sulfur (kg ha^{-1} year^{-1}) distribution for the period 2018 – 2019.

Using the data from the FCI 0018 project, we will determine the accounting of inputs and outputs in the S capture process conducted with the passive sampler through stoichiometric operations and material balances. Finally, we will validate the S concentrations obtained during the study period by performing stoichiometric calculations based on the principles mentioned above [34].

Experimental Part

Description of Reactions

To calculate the quantities of substances involved in or produced by the chemical reactions, we apply the principles of stoichiometry. This means that the total mass of the reactants must equal the total mass of the products. Using the data provided in **Table 4**, we determined the mass concentrations of S by applying Eq. (1) and considering the following reactions:

$$SO_3 + H_2O \rightarrow H_2SO_4 \quad (1)$$

$$H_2SO_4 + 2KCl \rightarrow K_2SO_4 + 2HCl\ K_2SO_4 + BaCl_2 \rightarrow BaSO_4 + 2KCl\ SO_4^{-2} + Ba^{2+} \rightarrow BaSO_4 \quad (2)$$

$$Fat = C/(Area \times P) \quad (3)$$

Where Fat is atmospheric deposition flux in kg ha^{-1} year^{-1}, C is the mass concentration of S (g), the Area is the external area of the funnel

Table 4. Sulfur (S) deposition flow data for 16 sites in the mangrove zone of El Salado, Guayaquil, Ecuador, from May 2018 to April 2019.

Sites	May	Jun	Jul	Aug	Sept	Oct	Nov	Dec	Jan	Feb	Mar	Apr
Trinitaria	0,02	2,01	3,42	3,42	4,83	6,93	4,28	4,28	3,98	1,35	4,57	3,10
Acacias	1,08	1,31	2,25	2,72	5,53	6,23	7,79	7,79	2,81	8,38	3,98	7,50
Pto. Guayaquil	6,23	2,25	17,01	2,01	6,70	7,87	4,57	4,57	2,81	3,69	6,62	5,74
Coguar	1,78	0,37	4,36	2,25	5,53	6,23	6,03	6,03	4,57	15,11	1,64	3,98
Floresta	1,31	1,55	11,62	4,83	5,76	6,47	3,69	3,69	3,10	3,10	2,23	4,57
Isla Santay	1,78	0,61	3,65	9,04	3,65	7,64	3,10	3,10	1,93	26,53	1,35	1,35
Primavera 1	5,29	4,59	1,78	6,23	2,95	2,95	7,79	7,79	2,81	1,64	1,93	1,64
El Recreo	0,61	1,31	4,12	2,72	3,89	4,36	3,10	3,10	2,52	3,10	5,74	3,98
San Eduardo	0,37	2,72	2,72	3,42	3,42	3,42	3,98	3,98	2,23	12,18	4,28	3,40
Par. Forestal	1,78	2,01	2,25	5,53	5,53	6,70	6,03	6,03	3,4	2,52	6,03	9,84
Inst.Inv.UG	0,84	1,08	3,89	3,89	2,48	2,48	5,74	5,74	1,93	3,10	3,10	6,62
Terranostra	4,12	1,31	3,65	1,78	2,95	2,25	2,81	2,81	1,93	1,05	1,35	2,52
Term. 3 Bocas	3,65	2,48	5,29	3,65	3,19	3,89	3,69	3,69	3,98	3,10	1,35	4,86
Pto. Hondo	2,25	0,84	1,08	2,48	2,25	2,72	2,81	2,81	4,28	2,23	0,47	4,86
Chongon	0,37	0,61	1,08	3,19	3,65	4,12	1,64	1,64	4,57	2,52	3,10	3,40
Col. Cenest	2,48	1,08	1,78	2,95	3,19	3,42	2,23	2,23	4,86	3,40	1,93	0,76

used in the passive sampler type throughfall (Project FCI 0018) or the collection of atmospheric deposition, and P is the period in years in which the passive sampler stays in the study place. The calculation for Eq. (3) is shown below:

$$F_{at} = 4.28 \text{ kg ha}^{-1} \text{ year}^{-1}$$

$$F_{at} = C/(\text{Area} \times P)$$

$$4.28 \text{ kg ha}^{-1} \text{ year}^{-1} = C/(4.15 \times 10^{-6} \text{ ha} \times 0.08 \text{ years})$$

$$C = 4.28 \text{ kg ha}^{-1} \text{ year}^{-1} \times 4.15 \times 10^{-6} \text{ ha} \times 0.08 \text{ years}$$

$$C = 1.42 \times 10^{-6} \text{ kg} = 1.42 \times 10^{-3} \text{ g}$$

Through this data, a retrospective analysis is conducted to determine the amount of contaminant in grams that has entered to the sampler, as follows:

$$SO_4^{-2} + Ba^{2+} \rightarrow BaSO_4 \quad (4)$$

The SO_4^{-2} reacts with the barium ion (Ba^{2+}), as shown in Eq. (4), to form barium sulfate ($BaSO_4$). The mass of sulfate in the original sample is then determined from the mass of $BaSO_4$ precipitate using stoichiometric relationships (see **Table 5**).

Table 5. Equality of masses between barium sulfate ($BaSO_4$) and its reactants.

$SO_4^{-2} + Ba^{2+} \rightarrow BaSO_4$			
	$BaSO_4$	SO_4^{-2}	Ba^{2+}
Molecular weight (g mol^{-1})	233.38	96.06	137.32
Reaction (g)	1.42×10^{-3}	1.42×10^{4}	

As shown below in Eq. (5), potassium sulfate (K_2SO_4) and $BaCl_2$ react to produce $BaSO_4$, which is the focus of this study. In this process, you can determine the amount of SO_4^{2-} present. Although KCl is also produced, it is not relevant to this analysis and will not be considered.

$$K_2SO_4 + BaCl_2 \rightarrow BaSO_4 + 2KCl \quad (5)$$

Table 6. Amount of sulfates that react in the combination process.

$K_2SO_4 + BaCl_2 \rightarrow BaSO_4 + 2KCl$				
	K_2SO_4	$BaCl_2$	$BaSO_4$	KCl
Molecular weight (g mol^{-1})	174.259	208.23	233.38	74.5513
Reaction (g)	1.06×10^{-3}	1.27×10^{-3}	1.42×10^{-3}	9.07×10^{-4}

The precipitation of $BaSO_4$ is the cornerstone of the analytical method used to quantify SO_4^{2-} in the samples. As shown in Eq. (5), K_2SO_4 derived from the washing of the ion-exchange resin, reacts stoichiometrically with $BaCl_2$ to form an insoluble precipitate of $BaSO_4$ and KCl. Since $BaSO_4$ is easily quantified by turbidimetry, its mass is used to back-calculate the original sulfate content in the atmospheric deposit. Although KCl is also produced, it remains in solution and does not interfere with the measurement, therefore, it is not considered in the mass balance. The stoichiometric process from $BaSO_4$ to their precursor compounds (K_2SO_4, $BaCl_2$, and KCl) is detailed in Eqs. (6) to (13), this allows the accurate determination of the mass of each reactant involved in the reaction sequence.

$$1.42 \times 10^{-3} \text{ g } BaSO_4 \text{ (1 mol } BaSO_4/233.38 \text{ g mol}^{-1} \text{ } BaSO_4) = 6.08 \times 10^{-6} \text{ mol } BaSO_4 \quad (6)$$

$$6.08 \times 10^{-6} \text{ mol } BaSO_4 \text{ (1 mol } K_2SO_4/(1 \text{ mol } BaSO_4) = 6.08 \times 10^{-6} \text{ mol } K_2SO_4 \quad (7)$$

$$6.08 \times 10^{-6} \text{ mol } K_2SO_4 \text{ (174.259 g mol}^{-1} K_2SO_4/1 \text{ mol } K_2SO_4) = 1.06 \times 10^{-3} \text{ g } K_2SO_4 \quad (8)$$

$$6.08 \times 10^{-6} \text{ mol } BaSO_4 \text{ (2 mol KCl/1 mol } BaSO_4) = 1.22 \times 10^{-5} \text{ mol KCl} \quad (9)$$

$$1.22 \times 10^{-5} \text{ mol KCl (74.5513 g mol}^{-1} \text{ KCl/1 mol KCl)} = 9.07 \times 10^{-4} \text{ g KCl} \quad (10)$$

$$6.08 \times 10^{-6} \text{ mol } BaSO_4 \text{ (1 mol } BaCl_2/1 \text{ mol } BaSO_4) = 6.08 \times 10^{-6} \text{ mol } BaCl_2 \quad (11)$$

$$6.08 \times 10^{-6} \text{ mol } BaSO_4 \text{ (1 mol } BaCl_2/1 \text{ mol } BaSO_4) = 6.08 \times 10^{-6} \text{ mol } BaCl_2 \quad (12)$$

$$6.08 \times 10^{-6} \text{ mol } BaCl_2 \text{ (208.23 g mol}^{-1} BaCl_2/1 \text{ mol } BaCl_2) = 1.27 \times 10^{-3} \text{ g } BaCl_2 \quad (13)$$

In the second reaction of the procedure, as shown below, H_2SO_4 reacts with KCl, which was used as a washing medium for the resin in the samplers. This reaction produces K_2SO_4 and HCl. HCl is released into the atmosphere, so it is not included in the analysis (see **Table 7**).

$$H_2SO_4 + 2KCl \rightarrow K_2SO_4 + 2HCl \quad (14)$$

Table 7. Detailed overview of the reaction between potassium sulfate (K_2SO_4) and hydrochloric acid (HCl).

$H_2SO_4 + 2KCl \rightarrow K_2SO_4 + 2HCl$				
	H_2SO_4	KCl	K_2SO_4	HCl
Molecular weight (g mol^{-1})	98.07	74.55	174.25	36.46
Reaction (g)	5.96×10^{-4}	9.07×10^{-4}	1.06×10^{-3}	4.44×10^{-4}

During the washing step of the ion-exchange resin, H_2SO_4 —originally formed from atmospheric SO_3 captured in the samplers— reacts with KCl, which is used as the eluent solution. As shown in Eq. (14), this neutralization reaction produces K_2SO_4 and HCl. The K_2SO_4 remains in solution and serves as the precursor for the subsequent precipitation of $BaSO_4$, the compound measured in the spectrophotometric analysis. In contrast, HCl is a volatile byproduct that either remains dissolved or partially evaporates under ambient conditions and does not interfere with the sulfate quantification; therefore, it is excluded from the final mass balance. The stoichiometric process from K_2SO_4 back to H_2SO_4 and KCl is detailed in Eqs. (15) to (21), this enables the precise reconstruction of the original sulfate mass captured by the passive samplers.

$$1.06 \times 10^{-3} \text{ g } K_2SO_4 \text{ (1 mol } K_2SO_4/174.259 \text{ } K_2SO_4) = 6.08 \times 10^{-6} \text{ mol } K_2SO_4 \quad (15)$$

$$6.08 \times 10^{-6} \text{ mol } K_2SO_4 \text{ (1 mol } H_2SO_4/1 \text{ mol } K_2SO_4) = 6.08 \times 10^{-6} \text{ mol } H_2SO_4 \quad (16)$$

$$6.08 \times 10^{-6} \text{ mol } H_2SO_4 \text{ (98.07 g } H_2SO_4/1 \text{ mol } H_2SO_4) = 5.96 \times 10^{-4} \text{ g } H_2SO_4 \quad (17)$$

$$6.08 \times 10^{-6} \text{ mol } K_2SO_4 \text{ (2 mol HCl/1 mol } K_2SO_4) = 1.22 \times 10^{-5} \text{ mol HCl} \quad (18)$$

$$6.08 \times 10^{-6} \text{ mol } K_2SO_4 \text{ (2 mol KCl/1 mol } K_2SO_4) = 1.22 \times 10^{-5} \text{ mol KCl} \quad (19)$$

$$1.22 \times 10^{-5} \text{ mol HCl (36.46 g HCl/1 mol HCl)} = 4.44 \times 10^{-4} \text{ g HCl} \quad (20)$$

$$1.22 \times 10^{-5} \text{ mol KCl (74.55 g KCl/1 mol KCl} = 9.07 \times 10^{-4} \text{ g KCl} \quad (21)$$

The reaction below illustrates how sulfur trioxide (SO_3), which falls from the atmosphere and is captured by samplers, reacts with water (H_2O), used as a washing medium to form H_2SO_4 (see **Table 8**).

$$SO_3 + H_2O \rightarrow H_2SO_4 \quad (22)$$

Table 8. Reaction of sulfur trioxide (SO_3) with water.

$SO_3 + H_2O \rightarrow H_2SO_4$			
	SO_3	H_2O	H_2SO_4
Molecular weight (g mol^{-1})	80.06	18.01	98.07
Reaction (g)	4.87×10^{-4}	1.10×10^{-4}	5.97×10^{-4}

Upon atmospheric deposition, SO_3 —the oxidation product of SO_3 emitted by industrial and vehicular sources— is captured by the passive samplers and subsequently hydrolyzed during the washing process. As shown in Eq. (22), SO_3 reacts rapidly with H_2O to form H_2SO_4, a stable and quantifiable compound that serves as the analytical precursor for sulfate determination. This reaction is critical because it converts a highly reactive gas (SO_3) into a soluble acid that can be retained by the ion-exchange resin and eluted for laboratory analysis. The stoichiometric relationship between SO_3 and H_2SO_4 is 1:1, enabling the back-calculation of the original atmospheric SO_3 mass from the measured H_2SO_4 (or ultimately $BaSO_4$) mass. The detailed mass balance for this step is presented in Eqs. (23) to (27), confirming that the experimentally observed H_2SO_4 mass (5.97×10^{-4} g) corresponds to 4.87×10^{-4} g of SO_3 originally captured by the sampler.

$$5.97 \times 10^{-4} \text{ g } H_2SO_4 \text{ (1 mol } H_2SO_4/98.07 \text{ g } H_2SO_4) = 6.08 \times 10^{-6} \text{ mol } H_2SO_4 \quad (23)$$

$$6.08 \times 10^{-6} \text{ mol } H_2SO_4 \text{ (1 mol } SO_3/1 \text{ mol } H_2SO_4) = 6.08 \times 10^{-6} \text{ mol } SO_3 \quad (24)$$

$$6.08 \times 10^{-6} \text{ mol } SO_3 \text{ (80.06 g SO\_3/1 mol } SO_3) = 4.87 \times 10^{-4} \text{ g } SO_3 \quad (25)$$

$$6.08 \times 10^{-6} \text{ mol } H_2SO_4 \text{ (1 mol } H_2O/1 \text{ mol } H_2SO_4) = 6.08 \times 10^{-6} \text{ mol } H_2O \quad (26)$$

$$6.08 \times 10^{-6} \text{ mol } H_2O \text{ (18.01 g } H_2O/1 \text{ mol } H_2O) = 1.10 \times 10^{-4} \text{ g } H_2O \quad (27)$$

Material Balance

To calculate the material balance for the process, we define the system by considering the flows involved, including the relevant variables and the occurrence of chemical reactions. Additionally, a material balance for each reactant involved in these reactions is provided, detailing the amount (in grams) of each reactant that enters, exits, is consumed, or is generated in the process.

The sampler is regarded as a reactor that contains an ion exchange resin, which is responsible for retaining the contaminating materials that are the focus of this study. This analysis allows the proposal of systems in which the inputs and outputs are evaluated based on the reactions outlined in the project. Two systems were identified. The first system involves the sampler during a washing process with H_2O and KCl. In this step, the sample reacts with both, and the corresponding analysis is conducted (as shown in **Figure 6**). For the washing procedure, 100 mL (100 g) of H_2O was added, followed by a second wash using 149.1 g of KCl, as noted in **Table 9**.

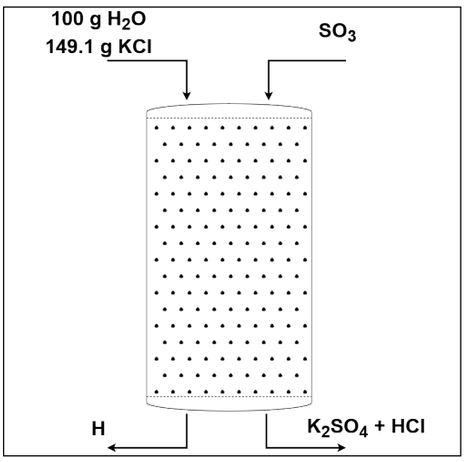

Figure 6. Flow diagram of the sampler washing process: hydrolysis of SO_3 to H_2SO_4 and elution with KCl to form K_2SO_4.

Table 9. Reactions observed when samplers were washed with distilled water (H_2O).

$SO_3 + H_2O \rightarrow H_2SO_4$			
	SO_3	H_2O	H_2SO_4
Molecular weight (g mol^{-1})	80.06	18.01	98.07
Input (g)	4.87×10^{-4}	100	0
Reaction (g)	4.87×10^{-4}	1.10×10^{-4}	0
output (g)	0	99.99	5.97×10^{-4}
Generating (g)	0	0	5.97×10^{-4}

The sampler is an open chemical reactor that contains an ion-exchange resin, which is responsible for retaining the atmospheric contaminants of interest in this study. This approach enables the definition of mass balance systems in which inputs and outputs are evaluated based on the chemical reactions occurring during the analytical procedure. Two sequential systems are considered. The first system corresponds to the washing step with distilled water, during which SO_3, previously captured from the atmosphere, undergoes hydrolysis. As shown in Eq. (22), SO_3 reacts stoichiometrically with H_2O to form H_2SO_4. For this step, 100 mL (100 g) of distilled H_2O was added to the sampler, as detailed in **Table 9**.

To verify mass conservation and ensure stoichiometric consistency, a material balance was applied to each chemical species involved. The general balance equation, derived from the law of conservation of mass, is expressed as:

$$\text{Output} = \text{Input} - \text{Reaction} + \text{Generating} \quad (28)$$

This equation states that the mass of a component leaving the system (Output) equals the initial mass introduced (Input) minus the amount consumed in the reaction (Reaction) plus any mass generated as a product (Generating). Applying Eq. (28) to the substances in the hydrolysis step yields the following results:

Eq. (29) shows that the output mass of H_2O is 99.99 g, indicating that only an insignificant fraction (1.10×10^{-4} g) is consumed in the reaction:

$$\text{Output } H_2O = 100 \text{ g} - 1.10 \times 10^{-4} \text{ g} + 0 = 99.99 \quad (29)$$

Eq. (30) confirms the complete consumption of the captured SO_3 with no residual mass remaining in the system:

$$\text{Output } SO_3 = 4.87 \times 10^{-4} \text{ g} - 4.87 \times 10^{-4} \text{ g} + 0 \text{ g} = 0 \text{ g} \quad (30)$$

Eq. (31) demonstrates that all H_2SO_4 present in the output is generated in situ, with no initial mass added:

$$\text{Output } H_2SO_4 = 0 \text{ g} - 0 \text{ g} + 5.97 \times 10^{-4} \text{ g} = 5.97 \times 10^{-4} \text{ g} \quad (31)$$

These results, showed in **Table 9**, validate the closed mass balance for the hydrolysis step and confirm the quantitative conversion of atmospheric SO_3 into measurable H_2SO_4, a critical prerequisite for the subsequent analytical stages of sulfate determination. In the second washing step, 149.1 g of KCl was used as the eluent solution. The H_2SO_4 generated in the first step reacts with KCl to produce K_2SO_4 and HCl, as shown in Eq. (14). **Table 10** presents the corresponding mass balance.

Table 10. Generation of reactions from washing samples with 2KCl.

$H_2SO_4 + 2KCl \rightarrow K_2SO_4 + 2HCl$				
	H_2SO_4	KCl	K_2SO_4	HCl
Molecular weight (g mol^{-1})	98.07	74.55	174.25	36.46
Input (g)	5.97×10^{-4}	149.1	0	0
Reaction (g)	5.97×10^{-4}	9.07×10^{-4}	0	0
Output (g)	0	149.09	1.06×10^{-3}	4.44×10^{-4}
Generating (g)	0	0	1.06×10^{-3}	4.44×10^{-4}

Applying the general balance of Eq. (28), Eq. (32) shows that the output mass of KCl is 149.09 g, indicating that only 9.07×10^{-4} g (an insignificant fraction) reacts:

$$\text{Output KCl} = 149.1 \text{ g} - 9.07 \times 10^{-4} \text{ g} + 0 = 149.09 \text{ g} \quad (32)$$

Eq. (33) confirms the complete consumption of H_2SO_4:

$$\text{Output } H_2SO_4 = 5.97 \times 10^{-4} \text{ g} - 5.97 \times 10^{-4} \text{ g} + 0 \text{ g} = 0 \text{ g} \quad (33)$$

Eq. (34) demonstrates that K_2SO_4 is entirely generated in situ, with no initial input:

$$\text{Output } K_2SO_4 = 0 \text{ g} - 0 \text{ g} + 1.06 \times 10^{-3} \text{ g} = 1.06 \times 10^{-3} \text{ g} \quad (34)$$

Eq. (35) shows the co-generated HCl, which remains in solution:

$$\text{Output HCl} = 0 \text{ g} - 0 \text{ g} + 4.44 \times 10^{-4} \text{ g} = 4.44 \times 10^{-4} \text{ g} \quad (35)$$

These results confirm the quantitative conversion of H_2SO_4 into K_2SO_4, enabling accurate sulfate determination via $BaSO_4$ precipitation.

The last analytical step involves the precipitation of sulfate as $BaSO_4$, which is quantified by turbidimetry. In this step, K_2SO_4 obtained from the previous elution with KCl reacts with $BaCl_2$ in a full-mix reactor, as shown in Eq. (5). **Table 11** summarizes the material balance for this precipitation system. A significant excess of BaClv (1 g) was used to ensure complete conversion of K_2SO_4 into the insoluble $BaSO_4$, which was then measured spectrophotometrically.

Table 11. Reaction between potassium sulfate (K_2SO_4) and barium chloride ($BaCl_2$).

$K_2SO_4 + BaCl_2 \rightarrow BaSO_4 + 2KCl$				
	K_2SO_4	$BaCl_2$	$BaSO_4$	KCl
Molecular weight (g mol^{-1})	174.25	208.23	233.38	74.55
Input (g)	1.06×10^{-3}	1	0	0
Reaction (g)	1.06×10^{-3}	1.27×10^{-3}	0	0
output (g)	0	1.00	1.42×10^{-3}	9.07×10^{-4}
Generating (g)	0	0	1.42×10^{-3}	9.07×10^{-4}

Applying the general material balance equation (Eq. 28), Eq. (36) shows that the output mass of $BaCl_2$ hasn't changed (1.00 g), as only 1.27×10^{-3} g is consumed:

$$\text{Output } BaCl_2 = 1.00 \text{ g} - 1.27 \times 10^{-3} \text{ g} + 0 = 1.00127 \text{ g} \quad (36)$$

Eq. (37) confirms the complete consumption of K_2SO_4:

$$\text{Output } K_2SO_4 = 1.06 \times 10^{-3} \text{ g} - 1.06 \times 10^{-3} \text{ g} + 0 \text{ g} = 0 \text{ g} \quad (37)$$

Eq. (38) demonstrates that $BaSO_4$ is entirely generated *in situ*:

$$\text{Output } BaSO_4 = 0 \text{ g} - 0 \text{ g} + 1.42 \times 10^{-3} \text{ g} = 1.42 \times 10^{-3} \text{ g} \quad (38)$$

Eq. (39) shows the co-generated KCl, which remains in solution and doesn't interfere with the turbidimetric measurement:

$$\text{Output KCl} = 0 \text{ g} - 0 \text{ g} + 9.09 \times 10^{-4} \text{ g} = 9.09 \times 10^{-4} \text{ g} \quad (39)$$

These results validate the stoichiometric completeness of the precipitation step and confirm that the mass of $BaSO_4$ measured directly reflects the original sulfate content captured from the atmosphere. The unquantified KCl is environmentally benign under analyti-

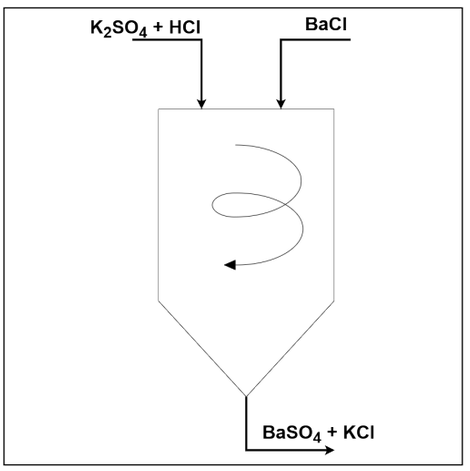

Figure 7. Flowchart of analytical precipitation: reaction of K_2SO_4 with $BaCl_2$ to form $BaSO_4$, the compound quantified by turbidimetry.

cal conditions and doesn't interfere in the final determination. This latter compound is released into the atmosphere, as illustrated in **Figure 7**.

$BaSO_4$ is the compound of interest because its mass is used to determine the amount of SO_4^{2-} originally present in the sample. Although the mass of SO_4^{2-} isn't equal to that of $BaSO_4$, it can be calculated using stoichiometric relationships based on their molecular weights, as shown in **Table 12**.

Table 12. Reaction between barium sulfate ($BaSO_4$) and sulfate ion (SO_4^{2-}).

$SO_4^{2-} + Ba^{2+} \rightarrow BaSO_4$			
	$BaSO_4$	SO_4^{2-}	Ba^{2+}
Molecular weight (g mol^{-1})	233.38	96.06	137.32
Reaction (g)	1.42×10^{-3}	5.85×10^{-4}	–

Eq. (4) shows the precipitation reaction. The insoluble precipitate is stable, easily measured by turbidimetry, and doesn't have environmental risks under laboratory conditions. As in the other reactions, KCl remains in solution and doesn't interfere with the analysis.

Results and Discussion

The SO_4^{2-} data, expressed in kg ha^{-1} $year^{-1}$, obtained during the period from 2018 to 2019, were converted into grams (**Table 13**) to facilitate the comparison of S mass in grams.

Table 13. Calculated sulfur trioxide (SO_3) and sulfate (SO_4^{2-}) values derived from stoichiometric calculations based on the exit data from the samplers at 16 different sites in the cities of Guayaquil and Durán during the period of 2018 to 2019.

Site/Seasons/g	SO_3 g		SO_4^{2-} g	
	Dry season (2018)	Rain season (2019)	Dry season (2018)	Rain season (2019)
San Eduardo	0.33	0.37	1.7×10^{-2}	1.06×10^{-3}
Acacias	0.49	0.64	1.36×10^{-3}	1.87×10^{-3}
Puerto de Guayaquil	0.73	0.53	1.36×10^{-3}	1.56×10^{-3}
COGUAR	0.46	0.70	1.36×10^{-3}	2.08×10^{-3}
Floresta 3	0.55	0.37	1.36×10^{-3}	1.08×10^{-3}
Isla Santay	0.46	0.88	1.36×10^{-3}	2.55×10^{-3}
Primavera 1	0.56	0.22	1.36×10^{-3}	6.35×10^{-3}
El Recreo	0.33	0.43	1.36×10^{-3}	1.26×10^{-3}
San Eduardo	0.34	0.62	1.36×10^{-3}	1.81×10^{-3}
Parque Forestal	0.51	0.62	1.36×10^{-3}	1.81×10^{-3}
Instituto de investigación	0.36	0.42	1.36×10^{-3}	2.67×10^{-3}
Terranostra	0.30	0.19	1.36×10^{-3}	1.99×10^{-3}
Terminal Tres Bocas	0.42	0.37	1.36×10^{-3}	1.08×10^{-3}
Puerto Hondo	0.24	0.33	1.36×10^{-3}	9.85×10^{-4}
Entrada de Chongón	0.23	0.38	1.36×10^{-3}	1.11×10^{-3}
Colegio Cenest Harvard	0.27	0.31	1.36×10^{-3}	9.08×10^{-4}

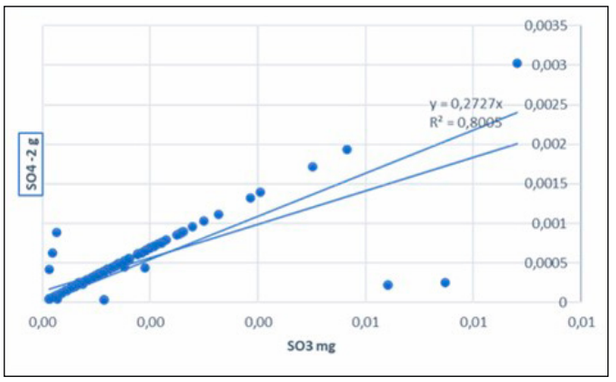

Figure 8. Normalization of sulfate ion (SO_4^{2-}) and sulfur trioxide (SO_3) data.

The SO_4^{-2} data collected in grams through stoichiometry and validated by mass balance are closely related to the SO_3 data obtained from the sampler throughfall (**Figure 8**).

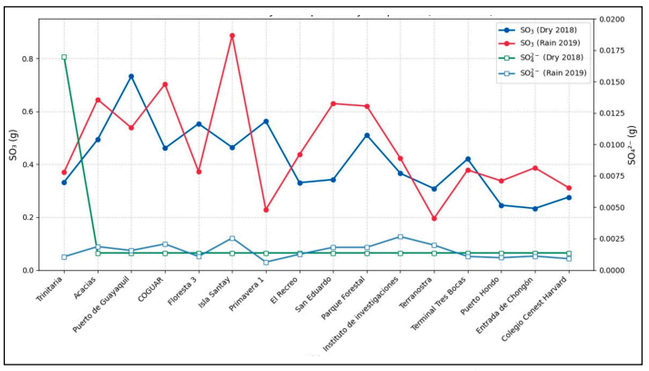

Figure 9. Distribution of sulfur trioxide (SO_3) and sulfate (SO_4^{2-}) concentrations during the dry and rainy seasons from 2018 to 2019.

We used stoichiometry to calculate the mass of SO_3 that fell to the ground and was captured by the Amberlite resin placed in the samplers. This resin is water-soluble and can oxidize in air without needing water droplets. The production of SO_3, as shown in **Figure 9**, is associated with shipping ports and its presence in nearby neighborhoods. It also results from thermoelectric power plants, industrial boilers, and various industries, including cement, glass, fiberglass, rock wool, ceramics, and metal foundries, as well as from the energy recovery of waste [34].

The passive sampler used for collection operates as an open system, allowing atmospheric matter to enter and exit through it. This sampler facilitates field operations to capture SO_4^{2-}. The system boundary is defined at the end of the sampler valve, which enables rainwater to escape from the system. In this context, the chemical process primarily involves quantifying the amount of each chemical component involved in various processes, including input, output, and usage. According to the law of conservation of mass, the total mass entering a process or unit is equal to the total mass exiting it. It is important to note that this principle refers to mass, not the quantity of matter measured in moles or to any other physical relationships among the components.

The presence of SO_2 in the atmosphere is closely linked to coal usage, contributing up to 50% of global emissions. The burning of fossil fuels also releases S, which constitutes about 2.3% of their composition. Once released, SO_2 dissolves in atmospheric water vapor to form acid rain, H_2SO_3, and H_2SO_4. The formation of these acids can persist for several days and involves several chemical reactions at different stages.

It's important to note that there are natural sources of SO_2, such as volcanic eruptions. For example, during the period from May to December 2018, the Cotopaxi volcano was active. The volcanic

plume demonstrated how SO_2 travelled following the predominant winds from the West (WNW-WSW) and carried the gases along this trajectory (see **Table 14**). This observation suggests a close relationship between the S concentrations determined in the present study and the high SO_2 values reported [35].

Table 14. Emissions from the Cotopaxi Volcano, Ecuador, 2018. Data for 2019 are not shown. Taken from [35].

Month (dry season)	Emission (t)	t/day	Daily average (t/day)	Wind direction
May	20,935	1682	675	West
June	17,603	1541	587	West
July	16,954	1532	547	West
August	12,002	738	387	Southwest
September	12,803	955	427	West
October	14,416	1171	465	Southwest
November	12,559	741	419	Southwest
December	29,487	1680	951	West

In the context of critical acidity loads for S, one of the levels assessed was the "mass balance" level, which involves calculating the chemical inputs and outputs of acidity per unit of time. The resulting critical load value was found to be 34%. This value is linked to the acidity levels in the ground and indicates potential risks for surrounding ecosystems [36]. Research suggests that agriculture, industry, and other activities significantly influence these levels. Consequently, this critical load value can serve as both a chemical criterion and an environmental indicator [37–38].

According to another study, combustion systems [39] require the presence of oxygen (O_2), which contributes to increase production of SO_2. These systems are commonly found in industrial settings, shipping areas, and some ways of transportation. As a result, the presence of SO_2 is associated with high concentrations in the study area. It is projected that the continued rise in energy demand will lead to ongoing contributions of SO_2 and nitrogen oxides (NOx) [40], which can manifest as acid rain. This phenomenon poses direct threats to the mangrove ecosystems surrounding the city of Guayaquil.

Conclusions

This study concludes that, following the release of contaminating materials into the atmosphere, SO_2 is formed upon initial contact with air. Due to the presence of O_2, SO_2 is subsequently converted to SO_3. This SO_3 is then collected by the passive sampler and absorbed by the Amberlite resin, which doesn't retain particulate materials that can be filtered. This finding is significant due to the phytotoxic effects associated with sulfite, highlighting a latent risk to local vegetation, particularly mangrove ecosystems.

It is important to note that critical load categories cannot be applied at the study site due to the lack of historical data or baseline assessments. Therefore, a level 0 classification is used, which provides a semi-quantitative approximation based on assigned critical load ranges for sensitive receptor ecosystems. Additionally, S inputs from volcanic sources are relevant to the outcomes of this study and represent another factor that may contribute to the deterioration of air quality in the port of Guayaquil and its surrounding urban and mangrove ecosystems.

To obtain better estimates of SO_2 fluxes and dry deposition, it is recommended to integrate modeling approaches with high-resolution meteorological data and spatial analysis of emission sources. Using passive sampling alongside active monitoring techniques (e.g., denuder systems or DOAS) may improve accuracy and temporal resolution. Furthermore, current modeled estimates of N deposition don't capture the full scope of reactive N inputs, particularly those from gaseous organic N species, nitrous acid (HONO), and nitric oxide (NO). Including these species in future monitoring campaigns would yield a more comprehensive understanding of N dynamics and their combined ecological impacts.

Acknowledgements

The Complementary Research Fund (FCI), registered under number 0018 at the University of Guayaquil, financed this research project titled "Relationship Between the Morphological Characteristics of Mangroves and SO2 Levels in the Area of the Main Port of Guayaquil, Province of Guayas, Ecuador".

References

[1] G. Morantes, G. Rincon, B. Jones, and A. Chanaba, "Addressing air quality challenges: Comparative analysis of Barcelona, Venezuela, and Guayaquil, Ecuador", *Heliyon*, vol. 10, no. 8, 2024. DOI: https://doi.org/10.1016/j.heliyon.2024.e29211%20.

[2] J. P. Solis Fonseca, L. C. Salazar Bravo, V. L. Romero Carrión, and A. d. l. A. Solís Salazar, "Congestión Vehicular y Contaminación Ambiental en Lima Metropolitana", *Revista Lasallista de Investigación*, vol. 19, no. 1, pp. 152–164, 2023. DOI: https://doi.org/10.22507/rli.v19n1a9.

[3] D. Xie, X. Ge, L. Duan, and J. Mulder, "Effects of acid deposition control in China: a review based on responses of subtropical forests", *Front. Enviroment. Science Engine*, vol. 18, no. 6, p. 77, 2024. DOI: https://doi.org/10.1007/s11783-024-1837-4.

[4] E. O. Robles, I. C. Silva, and S. J. B. Pulido, "Efectos del cambio climático en la gestión sostenible del recurso suelo", *Tecnociencia Chihuahua*, vol. 16, no. 3, pp. e1097, 2022. DOI: https://doi.org/10.54167/tch.v16i3.1097.

[5] R. M. Vázquez, Ma. G. Miranda Pascual, M. d. R. Romero Sánchez, and G. Muñoz Pérez, *Balance de materia y energía: procesos industriales*, México D.F., Grupo Editorial Patria, 2014.

[6] O. Quevedo, M. Calderón, D. Calle, and G. Montaño, "Análisis de los depósitos atmosfericos de azufre durante la época seca en Guayaquil, Ecuador", in *5th International Conference of Greening of Industry Network*, Mexico D.F., 2019.

[7] F. Macías Vázquez, M. Camps Arbestain, L. Rodríguez Lado, and E. Barreal Modroño, "Cargas críticas de contaminantes un criterio de evaluación de la sensibilidad de la naturaleza para la ordenación de actividades humanas", in *Reflexiones sobre el medio ambiente en Galicia*, Xunta de Galicia, Casares-Long, 2003.

[8] S. Schucht *et al.* "ETC/ATNI Report 04/2020: Costs of air pollution from European industrial facilities 2008–2017", 2021. [Online]. Available: https://www.eionet.europa.eu/etcs/etc-atni/products/etc-atni-reports/etc-atni-report-04-2020-costs-of-air-pollution-from-european-industrial-facilities-200820132017. [Last access: 05/01/2025].

[9] M. Kampa and E. Castanas, "Human health effects of air pollution", *Enviromental Pollution*, vol. 151, no. 2, pp. 362– 367, 2008. DOI: https://doi.org/10.1016/j.envpol.2007.06.012.

[10] J. Barberena and I. Hurtado, "Proceso de acidificación de las precipitaciones de Managua", *Revista Científica Estelí*, vol. 8, no. 31, 2019. DOI: https://doi.org/10.5377/farem.v0i31.8472.

[11] V. H. Lituma, A. Benavides, and L. K. Ninozca, "Plan de acción ambiental para prevenir la Contaminación Atmosférica en el Tráfico Marítimo en el Ecuador, caso Scrubber", *Centro Internacional de Investigación y Desarrollo*, pp. 242–258, vol. 3, no. 1. DOI: https://doi.org/10.46785/ciidj.v3i1.87.

[12] O. Quevedo *et al.*, "Referential seasonality of critical loads of sulfur on Rhizophora harrisonii in the port of Guayaquil", *WSEAS Transactions on Biology and Biomedicine*, vol. 15, pp. 24–34, 2018.

[13] O. P. Narayan, P. Kumar, B. Yadav, M. Dua, and A. K. Johri, "Sulfur nutrition and its role in plant growth and development", *Plant Signaling & Behavior*, vol. 18, no. 1, 2022. DOI: https://doi.org/10.1080/15592324.2022.2030082.

[14] G. Azuara-García, E. Palacios-Rosas, V. Palacios-Corte, and C. A. Rosas-Burgess, "Impactos potenciales de depósitos secos de SO2 en rendimientos de cultivos en México; una aproximación a escala nacional", *Agro productividad*, vol. 13, no. 6, 2020. DOI: https://doi.org/10.32854/agrop.vi.1678.

[15] R. Monsalvo Vázquez, M: G. Miranda Pascual, Ma. d. R. Romero Sánchez, and G. Muñoz Pérez, *Balance de materia y energía: procesos industriales*, México D.F., Patria, 2014.

[16] L. Darmstaedter and R. E. Oesper, "Jeremias Benjamin Richter", *Journal of Chemical Education*, vol. 5, no. 7, p. 785, 1928. DOI: https://doi.org/10.1021/ed005p785.

[17] P. J. Fito Suñer, M. L. Castelló Gómez, J. Tarrazo Morell, and M. Castro Giráldez, *Balances de materia y energía en ingeniería de bioprocesos*, Editorial Universitat Politècnica de València, 2023. Available: https://riunet.upv.es/handle/10251/198070.

[18] M. E. Fenn, M. A. Poth, and M. J. Arbaugh, "A Throughfall Collection Method Using Mixed Bed Ion Exchange Resin Columns", *Scientific World Journal*, vol. 15, pp. 122–130, 2002. DOI: https://doi.org/10.1100/tsw.2002.84.

[19] M. E. Fenn *et al.* "Ecological effects of Nitrogen deposition in the Western United States", Bioscience, vol. 53, no. 4, pp. 404–420. DOI: https://doi.org/10.1641/0006-3568(2003)053[0404:EEONDI]2.0.CO;2.

[20] Y. Zhao *et al.*, "Decline in bulk deposition of air pollutants in China Lags behind reductions in emissions", Nature Geoscience, vol. 15, pp. 190–195, 2023. DOI: https://doi.org/10.1038/s41561-022-00899-1.

[21] M.A. E. Vos, W. de Vries, G. F. Veen, M. R. Hoosbeek, and F. J. Sterck, "Testing ion exchange resin for quantifying bulk and throughfall deposition of macro- and micro-elements in forests", *Atmos. Meas. Tech*, vol. 17, pp. 6579–6594, 2024. DOI: https://doi.org/10.5194/amt-17-6579-2024.

[22] M. E. Fenn and M. A. Poth, "Monitoring nitrogen deposition in throughfall using ion exchange resin columns: A field test in the San Bernardino Mountains", *J. Environ. Qual.*, vol. 33, pp. 2007–2014, 2004. DOI: https://doi.org/10.2134/jeq2004.2007.

[23] S. Kohler, H. F. Jungkunst, C. Gutzler, R. Herrera, and G. Gerold, "Atmospheric Ionic Deposition in Tropical Sites of Central Sulawesi Determined by Ion Exchange Resin Collectors and Bulk Water Collector", *Water, Air & Soil Pollution*, vol. 223, pp. 4485–4494, 2012. DOI: https://doi.org/10.1007/s11270-012-1211-8.

[24] M. E. Fenn, A. Bytnerowicz, S. L. Schilling, and C. S. Ross, "Atmospheric deposition of nitrogen, sulfur and base cations in jack pine stands in the Athabasca Oil Sands Region, Alberta, Canada", *Environmental Pollution*, vol. 196, pp. 497–510, 2015. DOI: https://doi.org/10.1016/j.envpol.2014.08.023.

[25] W. G. Brumbaugh, J. W. Arms, G. L. Linder, and V. D. Melton, "Development of ion-exchange collectors for monitoring atmospheric deposition of inorganic pollutants in Alaska parklands", in *U.S. Geological Survey Scientific Investigations Report 2016–5096*, 2016. DOI: https://doi.org/10.3133/sir20165096.

[26] N. Clarke *et al.*, "Part XIV: Sampling and Analysis of Deposition, Version 2022-1" in *Manual on methods and criteria for harmonized sampling, assessment, monitoring and analysis of the effects of air pollution on forests*, Eberswalde, Thünen Institute of Forest Ecosystems, 2022. Available: https://www.icp-forests.org/pdf/manual/2020/ICP_Manual_part14_2022_Deposition_version_2022-1.pdf.

[27] Y. T. Fang *et al.*, "Nitrogen deposition and forest nitrogen cycling along an urban-rural transect in southern China", *Global Change Biol*, vol. 17, pp. 872–885, 2011. DOI: https://doi.org/10.1111/j.1365-2486.2010.02283.x.

[28] S. M. Simkin, D. N. Lewis, K. C. Weathers, G. M. Lovett, and K. Schwarz, "Determination of sulfate, nitrate and chloride in throughfall using ion.exchange resins", *Water, Air and Soil Pollution*, vol. 153, pp. 343–354, 2004. DOI: https://doi.org/10.1023/B:WATE.0000019958.59277.ed.

[29] H. Garcia-Gomez *et al.* "Atmospheric deposition of inorganic nitrogen in Spanish forests of Quercus ilex measured with ion-exchange resins and conventional collectors", *Environmental Pollution*, vol. 216, pp. 653–661, 2016. DOI: https://doi.org/10.1016/j.envpol.2016.06.027.

[30] P. Qian and J. Schoenau, "Practical applications of ion exchange resins in agricultural and environmental soil research", *Canadian Journal of Soil Science*, vol. 82, pp. 9–21, 2002. DOI: https://doi.org/10.4141/S00-091.

[31] S. Bayar, B. A. Fil, R. Boncukcuoglu, and A. E. Yilmaz, "Adsorption kinetics and isotherms for the removal of zinc ions from aqueous solutions by an ion-exchange resin", *Journal of the Chemical Society of Pakistan*, vol. 14, no. 4, pp. 841–848, 2012. Available: https://jcsp.org.pk/ArticleUpload/4697-21535-1-CE.pdf

[32] Secretaría de Comercio y Fomento Industrial, "Análisis de agua – Determinación del ion sulfato 1981", Norma Mexicana, NMX-AA-074-1981, 1981. [Online]. Available: https://agua.org.mx/wp-content/uploads/2011/01/nmx-aa-074-1981.pdf.

[33] D. K. C. Gurría, J. A. S. Canul, E. R. Lara, I. D. C. E. Cruz, I. D. Quintana, andR. M. C. Bretón, "Distribución espacio temporal del depósito atmosférico de nitrógeno en la ciudad de León Guanajuato durante la temporada de lluvias", in *Química e Ingeniería Verde para la sustentabilidad*, Universidad Autónoma de Nuevo León, México, 2022.

[34] G. Hérnandez-Gerónimo, J. R. Laines-Canepa, I. Ávila-Lázaro, R. Solís-Sílvan, and J. A. Sosa-Olivier, "Cálculos estequiométricos de factores de emisión para estimar emisiones fugitivas de gases de efecto invernadero en un centro de acopio de residuos sólidos", *Revista Internacional de Contaminación Ambiental*, vol. 38, pp. 165–179, 2022. DOI: https://doi.org/10.20937/rica.54024.

[35] Instituto Geofísico, "Informe anual de la emisión de SO2 del Volcán Cotopaxi 2018", Quito, 2018. Available: https://www.igepn.edu.ec/cotopaxi-gases/coto-ga/21916-informe-anual-emision-de-so2-cotopaxi-2018/file.

[36] Z. Yu et al., "Decline in bulk deposition of air pollutants in China Lags behind reductions in emissions", *Nature Geoscience*, vol. 15, pp. 190–195, 2023. DOI: https://doi.org/10.1038/s41561-022-00899-1.

[37] Z. Yu, D. Lei, L. Thorjorn, H. Lanhua, and H. Jiming, "Simultaneous assessment of deposition effects of base cations, sulfur, and nitrogen using and extended critical load function for acidification", *Environmental Science & Technology*, vol. 41, no. 6, 2007. DOI: https://doi.org/10.1021/es060380+.

[38] G. Xiaodong, Y. Qian, D. Lei, Z. Yu, P. Maximilian, and H. Jiming, "High-resolution maps of critical, for Sulfur and Nitrogen in China", *Scientific Data*, vol. 10, no. 339, 2023. DOI: https://doi.org/10.1038/s41597-023-02178-z.

[39] A. Sánchez, E. Eddings, and F. Mondragón, "Procesos para la captura de CO_2. Emisión de óxidos de nitrógeno y de azufre durante la oxi-combustión de un carbonizado", *Revista de la Academia Colombiana de Ciencias Exactas, Físicas y Naturales*, vol. 36, no. 138, pp. 115–123, 2012. DOI: https://doi.org/10.18257/raccefyn.36(138).2012.2438.

[40] P. Jigyasa, A. Shashi Bhushan, and A. Madhoolika, "Global Trends of Acidity in Rainfall and Its Impact on Plants and Soil", *Journal of Soil Science and Plant Nutrition*, vol. 23, pp. 398–419, 2023. DOI: https://doi.org/10.1007/s42729-022-01051-z.

Citación del artículo:

O. L. Quevedo Pinos, T. F. Alcívar Reyna, K. N. Zamora Murillo, R. M. Cerón Bretón, J. G. Cerón Bretón, A. R. Baque Onofre, and N. L. Veliz Saltos, "Stoichiometric Validation of Sulfur Sulfates in Guayaquil, Ecuador, during 2018 and 2019", *Rev. Colomb. Quim.*, vol. 54, no. 1, pp. 37–48, 2025. DOI: https://doi.org/10.15446/rev.colomb.quim.v54n1.119052.